Int J Adv Manuf Technol
DOI 10.1007/s00170-010-2791-3

ORIGINAL ARTICLE

Fibre laser welding of dissimilar alloys of Ti-6Al-4V and Inconel 718 for aerospace applications

Hui-Chi Chen · Andrew J. Pinkerton · Lin Li

Received: 10 February 2010 / Accepted: 15 June 2010

Abstract Challenges in dissimilar materials welding are the differences of physical and chemical properties between welding materials and the formation of intermetallic brittle phases resulting in the degradation of mechanical properties of welds. However, dissimilar materials welding is increasingly demanded from the industry as it can effectively reduce material costs and improve the design. In aerospace applications, Ti-6Al-4V titanium alloy and Inconel 718 nickel alloy have been widely used because of their superior corrosion resistance and mechanical properties. In this study, a single-mode continuous-wave fibre laser was used in butt welding of Ti-6Al-4V to Inconel 718. Investigations including metallurgical and mechanical examinations were carried out by means of varying processing parameters, such as laser power, welding speed and the laser beam offset position from the interface of the metals. Simple analytical modelling analysis was undertaken to explain the phenomena that occurred in this process. Results showed that the formation of intermetallic brittle phases and welding defects could be effectively restricted at welding conditions produced by the combination of higher laser power, higher welding speed and shifting the laser beam from the interface to the Inconel 718 alloy side. The amount of heat input and position of laser beam to improve the Ti-6Al-4V/Inconel 718 weld quality are suggested.

Keywords Fibre laser · Dissimilar material welding · Titanium alloy · Nickel alloy

H.-C. Chen (✉) · A. J. Pinkerton · L. Li
Laser Processing Research Centre, School of Mechanical, Aerospace and Civil Engineering, The University of Manchester, Sackville Street,
Manchester M60 1QD, UK
e-mail: Hui-Chi.Chen@postgrad.manchester.ac.uk

1 Introduction

Due to the excellent characteristics of good corrosion resistance, higher strength and creep resistance, titanium alloys like Ti-6Al-4V have been widely used in industry. One of the biggest applications of Ti-6Al-4V alloy is in the aerospace industries, for example as static and rotating components in the turbine engines [1]. Meanwhile, Inconel 718 nickel alloy, a high-temperature material, is also broadly used in the aerospace industries. Because of its superior mechanical properties and oxidation resistance at elevated temperatures, Inconel 718 is particularly suitable for manufactured components in the high temperature regions of aero engines and gas turbines [2, 3].

Today, the dissimilar materials welding process is increasingly attracting more attention in industry because it can reduce the material costs and improve the design flexibility. However, the formation of brittle phases, cracks and residual stresses still readily occur in a weld between dissimilar materials because their differences in physical and chemical properties, such as the melting and boiling points, thermal conductivity, density and coefficient of expansion [4]. A limited amount of systematic research in this area has been carried out until now. They were welding of aluminium alloy to steel [5]; aluminium alloy to titanium alloy [6]; copper to steel [7]; titanium alloy to stainless steel [8], dissimilar magnesium alloys [9] and dissimilar stainless steels [10]. Schubert et al. [11] pointed out that controlling the diffusion mechanism appropriately by applying a lower heat input can reduce the formation of brittle intermetallic phases in dissimilar materials welds. They obtained a better weld with a combination of a higher laser power and a higher welding speed in welding aluminium-steel and aluminium-magnesium joints. Using a high-energy density laser beam to restrict the amount of energy input was

Published online: 30 June 2010

another suggested method to control the heat diffusion and therefore minimise the thickness of the reactive interlayer and avoid the formation of brittle intermetallic phases especially in cases of welding steel-kovar, copper-steel and copper-aluminium joints [12]. Regarding the issue of different conductivities between welding materials, applying a backing block below welding samples has been pointed out as a method to control the heat flow and effectively suppress the thickness of the intermetallic layer in welding of steel to aluminium alloy [13].

Considering welding titanium and its alloys to nickel and its alloys: Seretsky and Ryba [14] used a Nd:YAG laser to investigate spot welding Ti to Ni with and without TiNi filler. Cracks and incompletely mixed liquids were observed in the welds. Chatterjee et al. [15, 16] butt welded Ti/Ni dissimilar materials using a CO_2 laser to investigate the solidification microstructure. They found that an asymmetric shape of weld, macrosegregation, and brittle intermetallic compounds, Ti_2Ni and $TiNi_3$, were readily generated within the weld with macroscopic cracks.

In the past 10 years, fibre lasers have been improved and developed intensively. Due to their advantages of good beam quality, low cost of maintenance and compact size, fibre lasers are suitable for most applications in laser materials processing and have been considered to compliment other types of laser systems, such as the Nd:YAG lasers and the CO_2 lasers [17]. Nowadays, fibre lasers have been increasing used in welding similar materials. For instance, fibre laser welding of steels [18], aluminium alloy [19, 20], stainless steel [21, 22], magnesium alloy [23, 24] and titanium alloy [25, 26]. Nevertheless, less work has been reported in this field related to fibre laser welding of dissimilar materials, such as welding of carbon steel to aluminium alloy [27] and titanium alloy to steel [28]. The purpose of this study is to investigate the influence of processing parameters on the weld quality in fibre laser welding of Ti-6Al-4V and Inconel 718. The melt pool shapes are modelled analytically using a two-dimensional model.

2 Experimental investigation

Sheets of Ti-6Al-4V and Inconel 718 with 2 mm thickness were laser butt welded together by a single mode fibre laser operating in the continuous wave mode. The chemical compositions and physical properties of these two materials are shown in Tables 1, 2 and Fig. 1, respectively.

Figure 2a shows the full setup of this experiment. An IPG 1 kW fibre laser with an emission wavelength of 1,070 nm was used. The spot diameter of the focused laser beam was approximately 72 μm with a Gaussian intensity distribution. During welding, argon was supplied co-axially and laterally as the shielding gas. Both Ti-6Al-4V and Inconel 718 samples for welding were 25×50×2 mm, as shown in Fig. 2b. The surface roughness of Ti-6Al-4V and Inconel 718 samples were, approximately, 4.66 and 4.36 Ra, respectively. Before welding, each sample was cleaned with acetone. The focal position of the laser beam was set at the top surface of the plates in this study.

Table 1 Chemical composition (wt.%) of Ti-6Al-4V and Inconel 718 [29, 30]

	Ti-6Al-4V	Inconel 718
Fe	0.40[a]	Balance
Al	5.5-6.75	0.20-0.80
V	3.5-4.5	–
Cr	–	17.2-21.0
Nb+Ta	–	4.75-5.50
Mo	–	2.80-3.30
Ti	Balance	0.65-1.12
Ni	–	50.0-55.0

[a] The maximum limit

A series of experiments was carried out to investigate the correlation of laser power, welding speed and the offset of the laser beam from the interface with the weld quality of full penetration welds. In Table 3, the one variable at a time method was used. Each trail was conducted a total of three times to ensure repeatability. Firstly, four levels of the laser power, 700, 800, 900 and 1,000 W, were tested at a fixed welding speed when the laser beam was positioned on the interface of samples to investigate the influence of the laser power on the weld quality. Next, a study of the effect of welding speed was carried out by using different welding speeds, 60, 80 and 100 mm/s at a fixed laser power of 1000 W. In the final experiment, three different offset positions of the laser beam—on the interface of samples, offset from the interface of samples to the Ti-6Al-4 V side 35 μm and offset from the interface of samples to the Inconel 718 side 35 μm—were tested while other parameters were kept constant to find the relation between the laser beam offset position and the weld quality.

After welding, all samples were sectioned across the weld, mounted in conductive resin, polished with diamond abrasives to 1 μm surface finish and etched with Krolls reagent for further examination. The weld bead shape including the weld width and depth were measured using optical microscopy with a personal computer running Solution DT software as shown in Fig. 3. The mean diameter of porosity and length of crack in welds were also observed and calculated from the cross-section of welds by optical microscopy. Microstucture and phenomena of microsegregation within welds were observed by means of optical microscopy and scanning electron microscopy equipped with backscattered electron imaging and energy

Table 2 Physical properties of Ti-6Al-4V and inconel 718

	Ti-6Al-4V [31, 33]	Inconel 718 [32, 34]
Hardness (Hv)	353	404
Melting point (°C)	1,655	1,260-1,336
Boiling point (°C)	3,315	2,917
Density (g/cm)	4.42	8.91
Specific heat (J/kg °C)	610	435
Coefficient of expansion (10^{-6} °C^{-1})	8.0	13.0
Latent heat (kJ/kg)	290	272
Solidus temperature (°C)	1,605	1,260
Liquidus temperature (°C)	1,655	1,336
Thermal conductivity (W/m°C)		
at 20°C	5.8	11.4
at ~T_m/2	17.5	21.3
Thermal diffusivity (m^2/s)		
at 20°C	2.15×10^{-6}	2.94×10^{-6}
at ~T_m/2	6.49×10^{-6}	5.50×10^{-6}

dispersive spectrometry. Profiles of microhardness including the base metals and the weld were tested using a Vickers microhardness machine with a 100 g load for 10 s. Figure 3 schematically illustrates evaluations of the weld dimension and the hardness distribution.

3 Experimental results

3.1 The weld geometry

As shown in Fig. 4, each full penetration weld has near-parallel sides under all the values of the laser power, welding speed and the laser beam offset position used in the experiments. In each case, the weld profile on the Ti-6Al-4V side is straighter than on the Inconel 718 side. The weld geometries were obvious different between three different laser beam offset positions when laser power and welding speed were 800 W and 100 mm/s as shown in Fig. 4a, b and c, respectively. The weld with a bigger fusion zone was obtained when the laser beam was positioned on the Inconel 718 side, as shown in Fig. 4c. Meanwhile, in Fig. 4b, the weld with a clear undercut and a smaller fusion zone was obtained when the laser beam was positioned on the Ti-6Al-4V side.

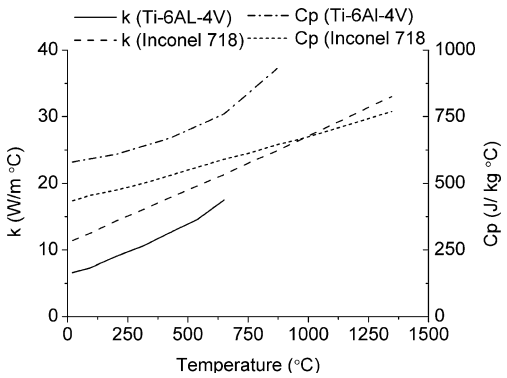

Fig. 1 Material properties of Ti-6Al-4V [31] and Inconel 718 [35] (Cp and *k* mean specific heat and thermal conductivity, respectively)

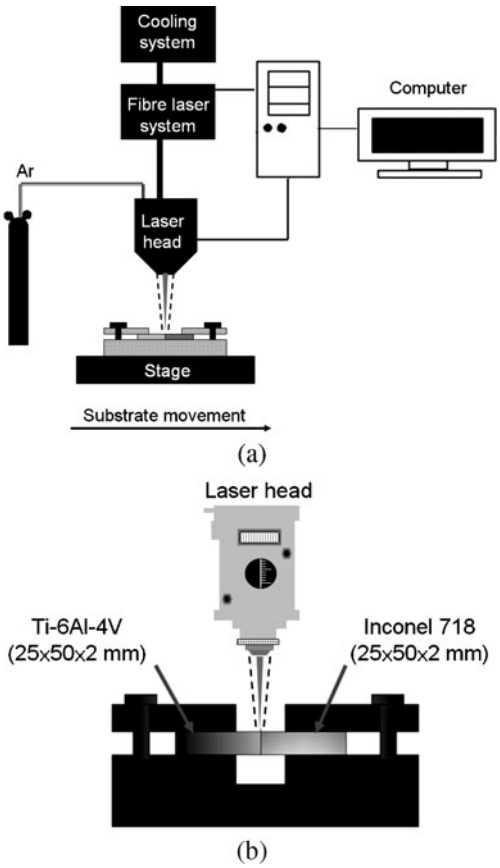

Fig. 2 Setup for the fibre laser welding of dissimilar materials process: (**a**) diagram of the full setup, (**b**) illustration of the clamped system

Table 3 Experimental matrix

Welding speed (mm/s)	Laser power (W)
60	700, 1,000[b]
80	700, 800, 900[b], 1,000[b]
100	700, 800[b], 900, 1,000[b]

[b] Three different laser beam offset positions—on the interface, offset from the interface to the Ti-6Al-4V side 35 μm and offset from the interface to the Inconel 718 side 35 μm—were carried out individually with these combinations of welding parameters

When the laser beam was positioned on the interface of samples, the relationship between the weld geometry, welding speed and laser power was shown in Fig. 5. When welding speed was kept at 80 and 100 mm/s, results show that, in both cases, the weld width randomly varied when laser power increased from 700 to 1,000 W as shown in Fig. 5a. Meanwhile, the influence of welding speed on the weld width with the constant laser power of 1,000 W was shown in Fig. 5b. The weld width decreased from 564 to 351 μm when welding speed was increased from 60 to 100 mm/s.

The relationship between the laser beam offset position and the weld width is shown in Fig. 6. When the laser power and welding speed were 900 W and 80 mm/s, respectively, a wider weld width of 603 μm was obtained when the laser beam was positioned on the interface. Meanwhile, the weld width with the laser beam offset to the Ti-6Al-4V side and the Inconel 718 side was around 495 and 458 μm, respectively. When laser power increased to 1,000 W, a narrower weld was found when the laser beam was positioned on the interface. A slightly wider weld was obtained when the laser beam was offset to the Ti-6Al-4V side.

3.2 The weld defects

The relationship between the formation of porosity, laser power, welding speed and the laser beam offset position is shown in Fig. 7. Porosity was produced at a wide range of parameter combinations, as shown in Fig. 7. The offset position of the laser beam probably was not the main factor to determine the formation of porosity. The diameter of micro-porosities observed from this work ranged from 15 to 172 μm. Figure 8 shows the relationship between the formation of crack, laser power, welding speed and the laser beam offset position. Cracks were produced at a wide range of parameter combinations as shown in Fig. 8. However, crack-free welds were more readily obtained at a higher laser power and a higher welding speed. As previously, the offset position of the laser beam was not a key factor to influence the formation of crack in the weld. The mean crack length in each weld was between 63 and 663 μm.

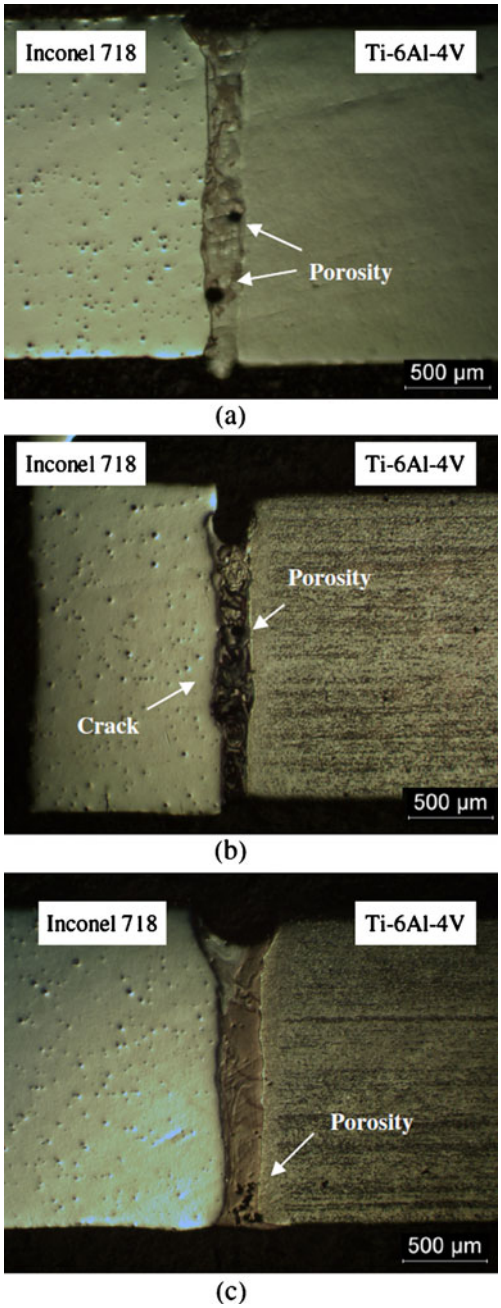

Fig. 4 Macrostructure of cross sections produced at 800 W and 100 mm/s when the laser beam was (**a**) positioned on the interface, (**b**) offset on the Ti-6Al-4V side, (**c**) offset on the Inconel 718 side

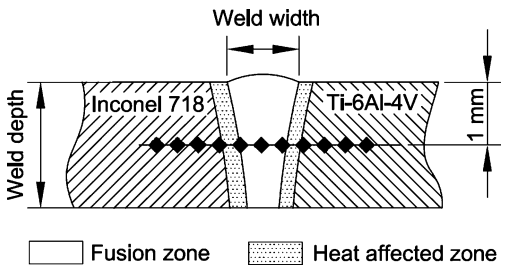

Fig. 3 Schematic diagram of the weld dimension and hardness tests

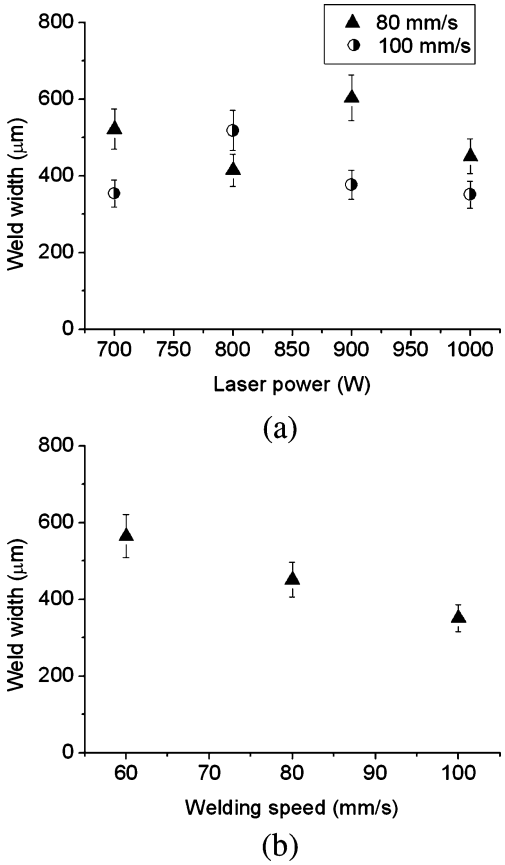

Fig. 5 Relationship between the weld width of full penetration welds and **a** different laser powers; **b** different welding speeds at a constant laser power of 1,000 W. (The laser beam was positioned on the interface of the welding materials)

3.3 Hardness distribution of the weld

Figure 9a shows the relationship between hardness distributions and laser power when the laser beam was positioned on the interface. It indicates that higher hardnesses occurred near the fusion zone in comparison with the parent materials. No clear trend was found between laser power and hardness variations. When laser power and the laser beam offset position were 700 W and on the interface, respectively, the influence of welding speed on hardness variations is shown in Fig. 9b. Results show that less hardness variations between the fusion zone and parent metals was obtained with the welding speed of 60 mm/s while more significant hardness variations were found at a higher welding speed of 80 or 100 mm/s.

Figure 10 displays the relationship between the laser beam offset position and hardness variations when laser power and welding speed were 900 W and 80 mm/s, respectively. Hardness variations near the fusion zone were clear when the laser beam were positioned on the interface or offset to the Ti-6Al-4V side as shown in Fig. 10a and b, respectively. On the other hand, in Fig. 10c, the hardness variation near the fusion zone was minimal when the laser beam was offset to the Inconel 718 side.

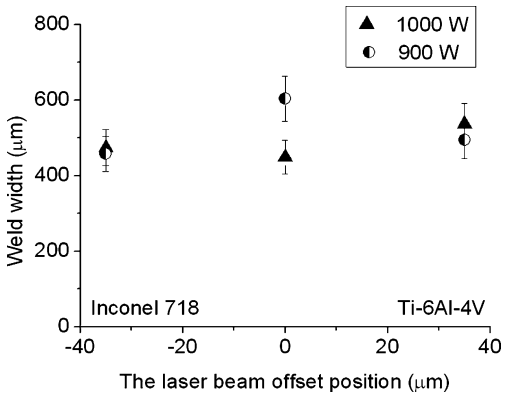

Fig. 6 Relationship between the weld widths and the laser beam offset position when welding speed was kept at 80 mm/s

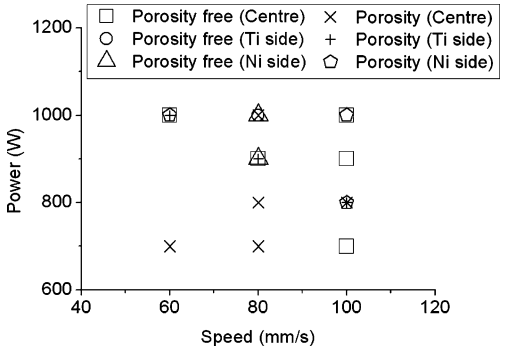

Fig. 7 Relationship between the formation of porosity, laser power, welding speed and the laser beam offset position. (Centre, Ti side and Ni side mean the laser beam was positioned on the interface, offset to the Ti-6Al-4 V side and offset to the Inconel 718 side, respectively)

3.4 Microsegregation of the weld

Welds produced at different welding conditions are shown in Fig. 11. Figure 11a is a partial cross-sectioned area

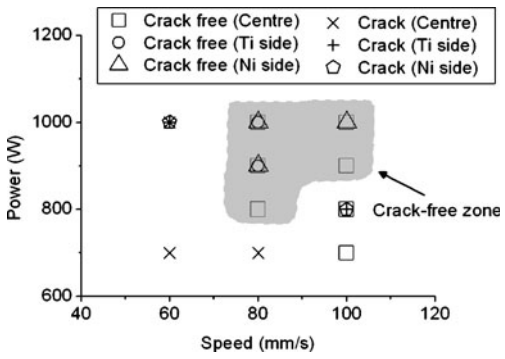

Fig. 8 Relationship between the formation of crack, laser power, welding speed and the laser beam offset position. (Centre, Ti side and Ni side mean the laser beam was positioned on the interface, offset to the Ti-6Al-4 V side and offset to the Inconel 718 side, respectively)

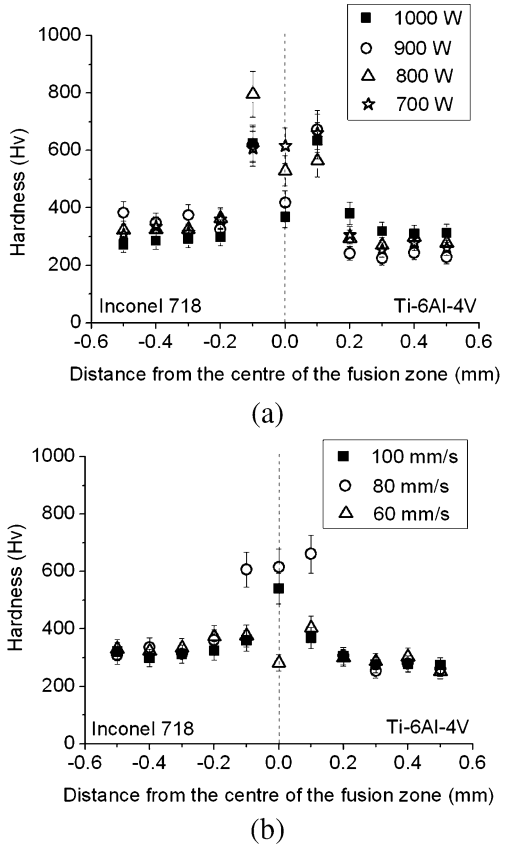

Fig. 9 Hardness distributions of welds produced at **a** the constant welding speed of 80 mm/s; **b** the constant laser power of 700 W

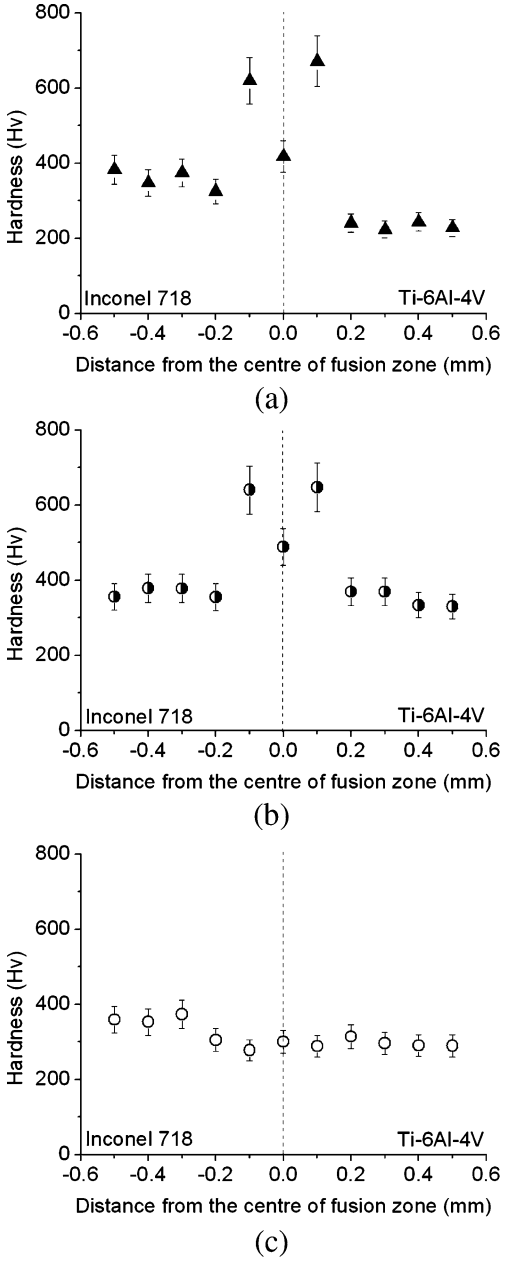

Fig. 10 Hardness distributions of welds produced at different laser beam offset positions when laser power and welding speed were 900 W and 80 mm/s, respectively, **a** on the interface, **b** offset to the Ti-6Al-4V side, **c** offset to the Inconel 718 side

observed under an optical microscope when welding conditions were 800 W, 60 mm/s and the laser beam was offset on the Inconel 718 side. It is likely that vortices occurred in the weld producing different microstructures. Hardness and chemical compositions of points A-G are tabulated in Tables 4 and 5, respectively. Higher hardnesses were obtained at points B, F and G. According to the Ni-Ti phase diagram [36] and their chemical compositions in Table 5, points B and G could be identified as the $TiNi_3$ phase. Meanwhile, point D with 814.1 Hv was classified as the TiNi phase and point A (263.5 Hv) and point E (375.4 Hv) are the hardness of unwelded Ti-6Al-4V and Inconel 718, respectively.

When welding conditions were 700 W, 80 mm/s and the laser beam was offset on the Ti-6Al-4V side, a back-scattered electron image near the top area of weld was taken and is shown in Fig. 11b. Because atomic number of Ni is higher than Ti, Ti-6Al-4V and Inconel 718 can be easily identified as the black and grey colour, respectively, in Fig. 11b. Several metal mixes were found within the weld. The molten material near the Ti-6Al-4V side was understandably richer in this alloy than that near the Inconel 718 side and clear vortices were found in the weld. Hardness at points H-M is listed in Table 4. A high hardness of 389.2 Hv occurred at point I.

4 Discussion

Usually, the formation of cracking can be discussed in terms of metallurgical and mechanical factors and previous research [15, 16] has highlighted two factors that could influence the formation of cracks within a Ti/Ni or Ti alloy/

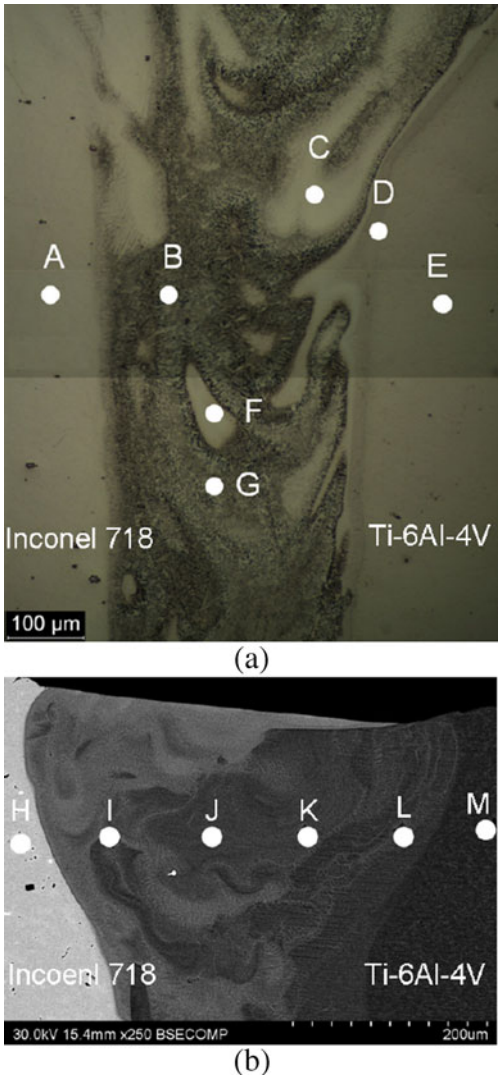

Fig. 11 Microsegregation of Ti-6Al-4V/Inconel 718 welds produced at **a** 800 W, 60 mm/s and the laser beam was offset to the Inconel 718 side (optical microscope image), **b** 700 W, 80 mm/s and the laser beam was offset to the Ti-6Al-4 V side; *SEM* backscattered electron image

Ni alloy weld. Firstly, two intermetallic brittle phases, Ti_2Ni and $TiNi_3$, which are readily produced within the weld during welding of a titanium alloy and a nickel alloy, can increase the susceptibility to failure at relatively low stresses. Secondly, the large differences of thermo-physical properties between Ti-6Al-4V and Inconel 718 can generate the stresses that actually cause the formation of cracks within the weld.

In order to clearly realise the relevance between processing parameters and the weld quality particularly in the formation of intermetallic brittle phases and cracks in welds, a simple two-dimensional analytical model was developed and compared with the experimental results. The model focuses on the relationships between laser power, welding speed, the laser beam offset position and the melt pool properties and behaviours, including the melt area, melt ratio and cooling rate.

Table 4 Hardness of points A-M in Fig. 9

	Hardness (Hv)
A	263.5
B	889.0
C	319.1
D	814.1
E	375.4
F	906.2
G	909.1
H	251.2
I	389.2
J	344.7
K	353.0
L	367.0
M	368.6

4.1 Analytical model for welding dissimilar materials

The thermal distribution in both Ti-6Al-4V and Inconel 718 welding plates were modelled individually according to Rosenthal's equation for two dimensional flow of heat [37] as shown in Eq. 1:

$$T(x,y) - T_0 = \frac{q'}{2\pi k} e^{-\lambda v x} K_0(\lambda v r) \quad (1)$$

where $T(x, y)$ is the temperature at point $(x, y$; °C), T_0 is the original sample temperature (20°C), q' is the rate of heat per unit length (W/m), k is the thermal conductivity (W/m °C), λ is the thermal diffusivity (m^2/s), v is welding speed (m/s), K_0 is the modified Bessel function of the second kind and zero order, and $r = (x^2 + y^2)^{1/2}$ is the distance from the heat source (m). In order to increase the precision of modelling results, values of thermal conductivity and thermal diffusivity at around half of the melting point of each material are used, as shown in Table 2 and Fig. 3. Heat transfer across the interface of the two welding materials is ignored at this stage. From results of the thermal distribution, the melt pool size is defined according to the melt points of Ti-6Al-4V (1,655ºC) and Inconel 718 (1,260ºC) as shown in Fig. 12a and b. In Fig. 12a, on the Ti-6Al-4V side, the melt pool width, the melt pool length in the forward direction and the melt pool length in the rear direction are presented as W_{Ti}, L_{1Ti} and L_{2Ti}, respectively. Meanwhile, in Fig. 12b, W_{Ni}, L_{1Ni} and L_{2Ni} are the melt pool width, the melt pool length in the forward direction and the melt pool length in the rear direction on the Inconel 718 side, respectively.

The Ti-6Al-4V and Inconel 718 melt pools are then taken as ellipses; one ellipse represents the area in front of

Table 5 Chemical composition (wt.%) of points A-G in Fig. 9a

	A	B	C	D	E	F	G
Ti	–	19.12	7.78	55.42	90.29	33.40	20.85
Al	–	–	–	–	5.50	2.31	–
V	–	–	–	3.50	4.21	–	–
Ni	55.27	44.39	50.62	25.05	–	35.06	45.59
Cr	21.36	17.23	18.72	6.00	–	12.72	18.26
Nb	–	4.84	4.72	–	–	–	–
Fe	17.42	14.42	16.18	7.28	–	11.23	15.30
Hg	5.95	–	–	–	–	5.28	–
S	–	–	1.98	–	–	–	–
Tm	–	–	–	3.74	–	–	–
Phase	Inconel 718	$TiNi_3$	Inconel 718	TiNi	Ti-6Al-4 V	Unknown	$TiNi_3$

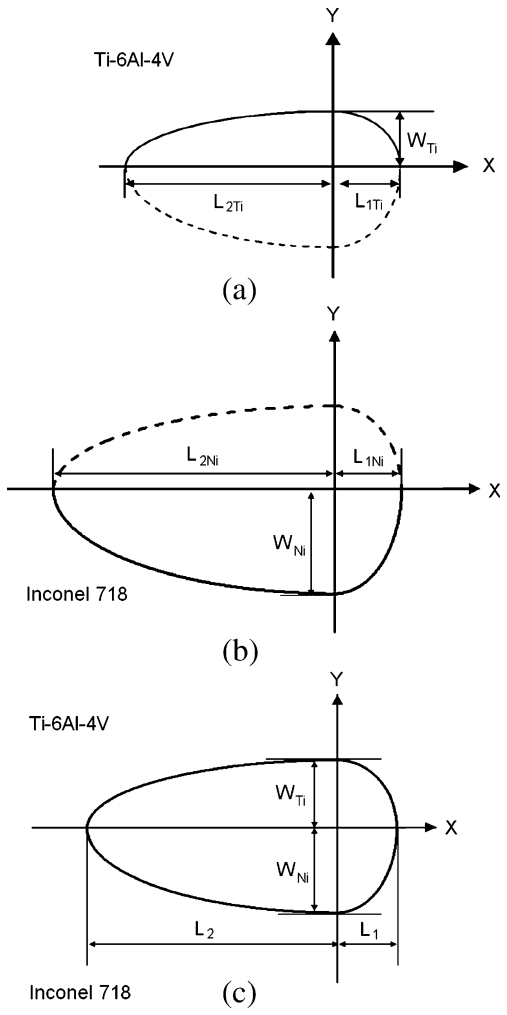

Fig. 12 Schematic diagram of the melt pool calculated according to Rosenthal's equation with characteristic dimensions shown: **a** the Ti-6Al-4V side, **b** the Inconel 718 side **c** the melt pool curve in laser dissimilar materials welding

the beam axis and one is the area behind the beam axis. The mean length of the separate melt pools in the forward and rear directions is $L_1 = \frac{(L_{1Ti}+L_{1Ni})}{2}$ and $L_2 = \frac{(L_{2Ti}+L_{2Ni})}{2}$, respectively. This is taken as the length of the combined pool. The melt pool is described in Eqs. 2a–2d and Fig. 12c:

On the Ti-6Al-4 V side ($y>0$):

$$\text{For } x > 0: \quad \frac{x^2}{{L_1}^2} + \frac{y^2}{W_{\text{Ti}}^2} = 1 \tag{2a}$$

$$\text{For } x < 0: \quad \frac{x^2}{{L_2}^2} + \frac{y^2}{W_{\text{Ti}}^2} = 1 \tag{2b}$$

On the Inconel 718 side ($y<0$):

$$\text{For } x > 0: \quad \frac{x^2}{{L_1}^2} + \frac{y^2}{W_{\text{Ni}}^2} = 1 \tag{2c}$$

$$\text{For } x < 0: \quad \frac{x^2}{{L_2}^2} + \frac{y^2}{W_{\text{Ni}}^2} = 1 \tag{2d}$$

After that, the melt pool area (mm^2), the melt ratio and the cooling rate of the melt pool (°C/mm) [38] are calculated as shown in Eqs. 3, 4, 5, respectively.

The melt pool area:

$$\text{Melt pool area} = \frac{\pi \times W_{Ti}(L_1 + L_2)}{4} + \frac{\pi \times W_{Ni}(L_1 + L_2)}{4} \tag{3}$$

The melt ratio:

$$\text{Melt ratio} = \frac{V_{\text{Ni}}}{V_{\text{Ti}}} = \frac{\frac{\pi \times W_{\text{Ni}}(L_1+L_2)}{4} \times t_{\text{Ni}}}{\frac{\pi \times W_{\text{Ti}}(L_1+L_2)}{4} \times t_{\text{Ti}}} \tag{4a}$$

where, V_{Ni}, V_{Ti}, t_{Ni} and t_{Ti} mean the melt volume in the Inconel 718 side and Ti-6Al-4 V side, and the thickness of the Inconel 718 and Ti-6Al-4 V plates, respectively. Due to

the same thickness of the Ti-6Al-4 V and Inconel 718 plates, Eq. 4a can be rewritten to Eq. 4b.

$$\text{Melt ratio} = \frac{W_{\text{Ni}}}{W_{\text{Ti}}} \tag{4b}$$

According to Hofmeister et al. [31], the cooling rate of a melt pool at the conductive cooling is related to the length of the pool by an expression of the form as shown in Eq. 5.

The cooling rate ($\dot{T}$):

$$\text{Log}\left(\dot{T}\right) = -2 \times \log(L_1 + L_2) + 3 \tag{5}$$

From the models it can be seen that when laser power and welding speed are kept at 1,000 W and 80 mm/s, a longer and bigger melt pool is obtained when the laser beam is offset to the Inconel 718 side as shown in Fig. 13a. Similar lengths of melt pool are obtained whether the laser beam is positioned on the interface or offset to the Ti-6Al-4V side. The melt area in the Inconel 718 side is slightly wider than in the Ti-6Al-4V side when the laser beam is positioned on the interface. A bigger melt area is found in the Ti-6Al-4V side when the laser beam is offset to the Ti-6Al-4V side. Similar trends are observed when welding speed increases from 80 to 100 mm/s, as shown in Fig. 13b.

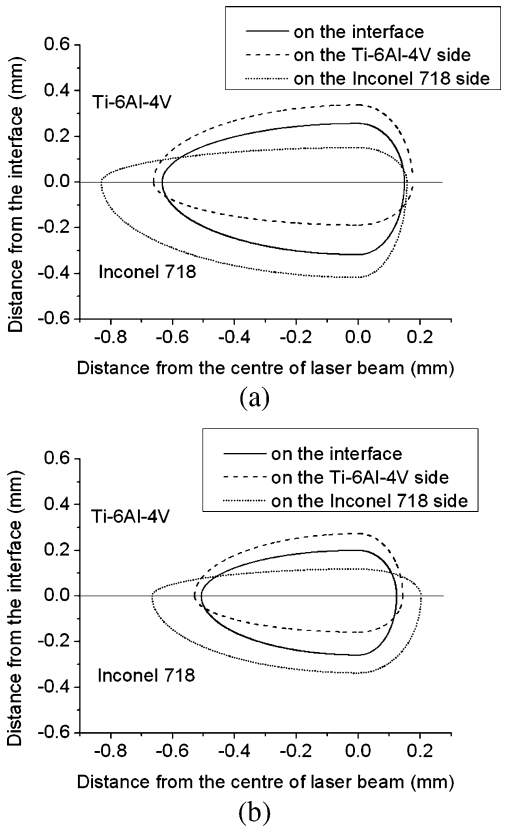

Fig. 13 The melt pool curves in fibre laser welding of Ti-6Al-4V to Inconel 718 obtained at three different laser beam offset positions with laser power of 1,000 W and welding speed of **a** 80 mm/s, **b** 100 mm/s

Relationships between the formation of cracks and the melt pool behaviours including the melt pool area, the melt ratio and the cooling rate are shown in Table 6 and Fig. 14. The cooling rate increases as the melt pool area decreases. There is a higher possibility to produce crack-free welds when the melt pool area and the cooling rate are in the range of 0.45~0.95 mm^2 and 1,142~3,423°C/sec, respectively. Welds with crack readily occur when the heat input is higher than 16 J/mm or lower than 9 J/mm. Crack-free welds with the smaller melt ratio (symbol "○") are observed within a very small processing window (the melt pool area and the cooling rate are around 0.44~0.59 mm^2 and 1,946~2,930°C/sec, respectively).

4.2 Discussion on experimental results

The amount of heat input can determine the degree of dilution and chemical composition in the weld [39]. It also determines the cooling rate, which is inversely proportional to the square of the melt pool length [38]. Thermal strains caused by high cooling rates can increase the crack initiation rate, but a higher thermal gradient resulting in a rapid cooling rate in the weld can also reduce the grain size to increase solidification crack resistance [40]. Additionally, a rapid cooling rate may induce non-equilibrium solidification in the weld and thus amount of segregation in the solidified pool [12, 41]. Modelled results (Fig. 14) indicate that crack-free welds were produced at a wide range of cooling rates so together these effects do not seem to be dominant in determining if cracking will occur in the fibre laser welding of Ti-6Al-4V to Inconel 718 process.

The melting ratio of fused materials is another important factor that determines the formation of defects in dissimilar materials welds [12]. Producing a bond similar to a brazed joint, by melting one material to induce another one to melt, has been suggested as a method to avoid the formation of intermetallic phases within the weld [4]. Perhaps because of this mechanism, the majority of the crack-free welds were produced at a higher melt ratio in Table 6 and Fig. 14. It is possible that when the beam was positioned on the Inconel 718 side, the lower melting point and higher thermal conductivity of Inconel 718 meant the heat could dissipate more quickly resulting in the lower thermal gradient and a wider fusion zone (Fig. 4c) than when on the Ti-6Al-4V side. Accordingly, the influence of the Marangoni forces on the melt pool surface could be less when the laser beam was positioned on the Inconel 718 side. For these reasons, the smaller hardness variation that occurred (Fig. 10c) indicates less formation of Ti-Ni intermetallics, which can increase strength and hardness but decrease ductility. Due to Ti-6Al-4V having a lower thermal conductivity than Inconel 718, when the laser beam was offset to the Ti-6Al-4V side, more heat could

Table 6 Detailed values from the analytical modelling with different welding parameters

Speed (mm/s)	Power (W)	Laser beam position[c]	Heat input (J/mm)	Melt pool area (mm^2)	Melt ratio	Cooling rate (°C/sec)	The formation of crack
60	700	Centre	11.67	0.39	1.27	4,625.16	Crack
60	1,000	Ti side	16.67	0.95	0.70	1,021.69	Crack
60	1,000	Centre	16.67	1.05	1.60	1,061.33	Crack
60	1,000	Ni side	16.67	1.35	3.60	689.49	Crack
80	700	Centre	8.75	0.21	1.26	9,268.46	Crack
80	800	Centre	10.00	0.30	1.46	5,405.81	Crack-free
80	900	Ti side	11.25	0.44	0.55	2,930.67	Crack-free
80	900	Centre	11.25	0.46	1.25	3,139.48	Crack-free
80	900	Ni side	11.25	0.59	2.98	1,860.01	Crack-free
80	1,000	Ti side	12.50	0.59	0.56	1,946.53	Crack-free
80	1,000	Centre	12.50	0.64	1.24	1,983.89	Crack-free
80	1,000	Ni side	12.50	0.83	2.76	1,142.71	Crack-free
100	700	Centre	7.00	0.16	1.24	1,0711.01	Crack-free
100	800	Centre	8.00	0.21	1.21	7,800.86	Crack-free
100	800	Ti side	8.00	0.22	0.50	6,055.21	Crack
100	800	Ni side	8.00	0.24	4.16	5,267.95	Crack
100	900	Centre	9.00	0.29	1.26	5,077.40	Crack-free
100	1,000	Centre	10.00	0.39	1.30	3,423.88	Crack-free
100	1,000	Ni side	10.00	0.51	2.85	1,933.88	Crack-free

[c] Centre, Ti side and Ni side mean the laser beam was positioned on the interface, offset to the Ti-6Al-4 V side and offset to the Inconel 718 side, respectively

accumulate in the Ti-6Al-4V side. This could have caused a narrower fusion zone (Fig. 4b), a higher thermal gradient and hence a strong Marangoni fluid flow, assisting the formation of the brittle intermetallic phases and increasing hardness variations, as indicated in Fig. 10b.

For optimum properties, it is important to avoid the formation of these intermetallic phases in the welds [42, 43]. In this case, it is possible to achieve this by appropriately restricting the size and extent of the melt pool and the solidification time. When the laser beam is offset to the Inconel 718 side, the significant reduction of the melt area in the Ti-6Al-4V side and the wider melt area in the Inconel 718 side (Fig. 13) may cause less vigorous convective flow in the molten zone around the keyhole, avoiding the formation of intermetallic phases in the weld because most of heat input can be lost quickly on the Inconel 718 side before enough heat is transferred into the Ti-6Al-4V side to induce severe microsegregation [44].

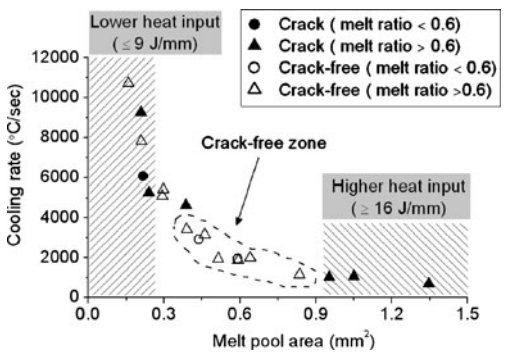

Fig. 14 Relationship between the formation of crack, the melt pool area, melt ratio and cooling rate

Crack-free welds were also readily observed at higher welding speed, as shown in Fig. 8. Although higher speed is normally related to higher cooling rate, any direct relation between cracking and cooling rate has already been considered. It is therefore likely that other factors apart from cooling rate and intermetallic formation played a secondary role in determining the final state of a weld. Melt pool geometry (elongation at higher speeds), keyhole geometry and stability effects and slight difference beam absorption at different traverse velocities may have contributed.

5 Conclusions

The effects of three processing parameters, laser power, welding speed and offset distance of the laser beam from the interface, were investigated individually during fibre laser welding of Ti-6Al-4V to Inconel 718. Experimental results indicated that when welding 2 mm thick sheets of

Ti-6Al-4V to Inconel 718 with an IPG 1 kW fibre laser, crack-free welds could be readily obtained by a higher laser power and welding speed. A better quality weld with less hardness variations and less chance of cracks can be generated by offsetting the laser beam approximately 35 μm from the interface to the Inconel 718 side and using a combination of a higher laser power and a higher welding speed. This is attributed to this method suppressing the formation of Ti-Ni intermetallic brittle phases.

Acknowledgement The UK Engineering and Physical Sciences Research Council (EPSRC) is acknowledged for grant EP/C013352/1, which allowed the purchase of the single mode, high-power fibre laser used here.

References

1. Boyer RR (1996) An overview on the use of titanium in the aerospace industry. Mater Sci Eng A 213:103–114
2. Smith WF (1993) Structure and properties of engineering alloys, 2nd ed. McGraw-Hill: New York
3. Gobbi S et al (1996) High powder CO_2 and Nd-YAG laser welding of wrought Inconel 718. J Mater Process Technol 56:333–345
4. Sun Z, Ion JC (1995) Laser-welding of dissimilar metal combinations. J Mater Sci 30:4205–4214
5. Torkamany MJ et al (2010) Dissimilar welding of carbon steel to 5754 aluminum alloy by Nd: YAG pulsed laser. Mater Des 31:458–465
6. Chen Y et al (2010) Influence of interfacial reaction layer morphologies on crack initiation and propagation in Ti/Al joint by laser welding-brazing. Mater Des 31:227–233
7. Yao C et al (2009) Interface microstructure and mechanical properties of laser welding copper–steel dissimilar joint. Opt Lasers Eng 47:807–814
8. Theron M et al. (2007) "CW Nd:YAG laser welding of dissimilar sheet metals," presented at the ICALEO 2007-26th International Congress on Applications of Laser and Electro-Optics
9. Kolodziejcak P, Kalita W (2009) Properties of CO_2 laser-welded butt joints of dissimilar magnesium alloys. J Mater Process Technol 209:1122–1128
10. Anawa EM, Olabi AG (2008) Control of welding residual stress for dissimilar laser welded materials. J Mater Process Technol 204:22–33
11. Schubert E et al (2001) Light-weight structures produced by laser beam joining for future applications in automobile and aerospace industry. J Mater Process Technol 115:2–8
12. Mai TA, Spowage AC (2004) Characterisation of dissimilar joints in laser welding of steel-kovar, copper-steel and copper-aluminium. Mater Sci Eng A 374:224–233
13. Borrisutthekul R et al (2007) Suppression of intermetallic reaction layer formation by controlling heat flow in dissimilar joining of steel and aluminum alloy. Mater Sci Eng A 467:108–113
14. Seretsky J, Ryba ER (1976) Laser-welding of dissimilar metals—titanium to nickel. Weld J 55:S208–S211
15. Chatterjee S et al (2006) Microstructure development during dissimilar welding: case of laser welding of Ti with Ni involving intermetallic phase formation. J Mater Sci 41:643–652
16. Chatterjee S et al (2008) Phase formation in Ti/Ni dissimilar welds. Mater Sci Eng A 490:7–15
17. Vollertsen F, Thomy C (2005) "Welding with fibre lasers from 200 to 17000 W," in ICALEO 2005—24th International Congress on Applications of Laser and Electro-Optics. Miami, FL, USA, pp 254–263
18. Quintino L et al (2007) Welding with high power fiber lasers—a preliminary study. Mater Des 28:1231–1237
19. Katayama S et al (2009) Fibre laser welding of aluminium alloy. Weld Int 23:744–752
20. Nagayama H et al. (2007) Weld penetration and welding phenomena of aluminium alloy with high-power fibre laser. In Laser Materials Processing Conference, pp. 916-924
21. Katayama S, Kawahito Y (2009) Elucidation of phenomena in high-power fiber laser welding and development of prevention procedures of welding defects. Proc SPIE Int Soc Opt Eng 7195:71951R (9 pp.)
22. Kawahito Y et al (2007) Elucidation of high-power fibre laser welding phenomena of stainless steel and effect of factors on weld geometry. J Phys D Appl Phys 40:5854–5859
23. Yu L et al (2009) Weld porosity in fibre laser weld of thixomolded heat resistant Mg alloys. Sci Technol Weld Join 14:554–558
24. Sakai Y et al (2008) Fiber laser welding of noncombustible magnesium alloy. Advanced Welding and Micro Joining/Packaging for the 21st Century 580-582:479–482
25. Iammi J et al (2008) "Fibre laser welding of Ti6Al4V," in PICALEO 2008—3rd Pacific International Conference on Applications of Lasers and Optics. Beijing, China, pp 152–157
26. Costa A et al (2007) Analysis of beam material interaction in welding of titanium with fiber lasers. Mater Manuf Process 22:798–803
27. Ozaki H, Kutsuna M (2009) Laser-roll welding of a dissimilar metal joint of low carbon steel to aluminium alloy using 2 kW fibre laser. Weld Int 23:345–352
28. Park SJ et al (2008) "Dissimilar metal welding titanium and steel sheet by fiber laser," in PICALO 2008—3rd Pacific International Conference on Applications of Lasers and Optics. Beijing, China, pp 158–162
29. ASTM Standard B637 (2003) Specification for precipitation-hardening nickel alloy bars, forgings, and forging stock for high-temperature service
30. ASTM Standard B265 (2008) Specification for titanium and titanium alloy strip, sheet, and plate
31. Boyer R (1994) Materials properties handbook: titanium alloys. ASM International
32. Gale WF, Totemeier TC (2004) Smithells metals reference book, 8th ed. Elsevier
33. Boivineau M et al (2006) Thermophysical properties of solid and liquid Ti-6Al-4V (TA6V) alloy. Int J Thermophys 27:507–529
34. Kermanpur A et al (2004) "Effect of process parameters on grain structure formation during VAR of Inconel alloy 718," presented at the Proceedings of the 2003 International Symposium on Liquid Metals. Nancy, France
35. Manson S (1968) Nonferrous alloys. Revised, March
36. Thaddeus HO, Massalski B. In: Subramanian PR, Kacprzak L (eds.) Binary alloy phase diagrams, Vol. 3, 2nd ed: ASM International, Materials Park, Ohio
37. Rosenthal DT (1946) The theory of moving sources of heat and its applications to metal treatments. ASME 48:846–866
38. Hofmeister W et al (2001) Solidification in direct metal deposition by LENS processing. JOM 53:30–34
39. Lancaster JF (1999) Metallurgy of Welding, 6th ed. Woodhead Publishing
40. Zhao H et al (1999) Current issues and problems in laser welding of automotive aluminum alloys. Int Mater Rev 44:238–266
41. Debroy T, David SA (1995) Physical Processes in fusion welding. Rev Mod Phys 67:85–112
42. Smallman RE, Bishop RJ (1999) Modern physical metallurgy and materials engineering. Elsevier Science, Process, Applications
43. Böllinghaus T, Herold H (2005) Hot cracking phenomena in welds. Springer: Berlin
44. Kou S (2002) Welding metallurgy, 2nd ed. A Wiley-Interscience Publication